Methane Steam Reforming at Microscales: Operation Strategies for Variable Power Output at Millisecond Contact Times

Georgios D. Stefanidis and Dionisios G. Vlachos
Dept. of Chemical Engineering and Center for Catalytic Science and Technology (CCST), University of Delaware, 150 Academy Street, Newark, DE 19716

Niket S. Kaisare
Dept. of Chemical Engineering and Center for Catalytic Science and Technology (CCST), University of Delaware, 150 Academy Street, Newark, DE 19716, and Dept. of Chemical Engineering, Indian Institute of Technology - Madras, Chennai 600-036, India

Matteo Maestri
Dept. of Chemical Engineering and Center for Catalytic Science and Technology (CCST), University of Delaware, 150 Academy Street, Newark, DE 19716, and Dipartimento di Chimica, Materiali e Ingegneria Chimica "Giulio Natta", Politechnico di Milano, Piazza Leonardo da Vinci 32, Milano, 20133, Italy

DOI 10.1002/aic.11672
Published online November 14, 2008 in Wiley InterScience (www.interscience.wiley.com).

The potential of methane steam reforming at microscale is theoretically explored. To this end, a multifunctional catalytic plate microreactor, comprising of a propane combustion channel and a methane steam reforming channel, separated by a solid wall, is simulated with a pseudo 2-D (two-dimensional) reactor model. Newly developed lumped kinetic rate expressions for both processes, obtained from a posteriori *reduction of detailed microkinetic models, are used. It is shown that the steam reforming at millisecond contact times is feasible at microscale, and in agreement with a recent experimental report. Furthermore, the attainable operating regions delimited from the materials stability limit, the breakthrough limit, and the maximum power output limit are mapped out. A simple operation strategy is presented for obtaining variable power output along the breakthrough line (a nearly* iso-flow rate ratio line*), while ensuring good overlap of reaction zones, and provide guidelines for reactor sizing. Finally, it is shown that the choice of the wall material depends on the targeted operating regime. Low-conductivity materials increase the methane conversion and power output at the expense of higher wall temperatures and steeper temperature gradients along the wall. For operation close to the breakthrough limit, intermediate conductivity materials,*

Correspondence concerning this article should be addressed to D. Vlachos at vlachos@udel.edu.

such as stainless steel, offer a good compromise between methane conversion and wall temperature. Even without recuperative heat exchange, the thermal efficiency of the multifunctional device and the reformer approaches ~65% and ~85%, respectively.
 AIChE J, 55: 180–191, 2009
Keywords: steam reforming, catalytic combustion, microreactors, methane, propane, hydrogen, syngas, multifunctional

Introduction

Steam reforming (SR) of hydrocarbons is still the principal industrial process for hydrogen production in refineries and petrochemical plants. The hydrocarbon feedstock can range anywhere between natural gas to naphtha feeds. An overview of the industrial developments in the SR process is given by Rostrup-Nielsen.[1,2] Nowadays, the increased interest in hydrogen, as an alternative to transportation and stationary power fuels, has rendered the SR process a key element for the hydrogen economy worldwide.[3] At the industrial level, SR, an endothermic process, is taking place in tubular reactors positioned in large gas fired furnaces. The process gas is heated up to the reaction temperature by means of radiation from the flue gases and the furnace walls. The process is relatively slow since the residence time is on the order of seconds.[4] It is also rather bulky, because of the space required to accommodate the flames in the furnace, and typically with low thermal efficiency, since typically only half of the heat produced in the furnace is transferred to the tubes. Because of these downsides, SR at micro- and mesoscales has received increased attention over the last 15 years. Currently, SR downscaling is a pressing topic of research in light of potential hydrogen utilization in various daily life applications, such as portable devices (e.g., cell phones, laptops), transportation, or local power stations (buildings, farms).[5,3]

Experimental work on methane SR in microreactors has been reported in[6,7,4]. Venkataraman et al.[4] studied combined catalytic methane combustion on Pt and steam methane reforming on Rh in mesoscale catalytic plate reactors (CPR).[4] They reported self-sustained and stable operation for several hours without deactivation, as well as high-methane conversion (>95%), with a residence time ~70 ms. Tonkovich and coworkers described methane SR on a Rh/MgO catalyst in a single channel microreactor with adjacent cylindrical tubes for catalytic hydrogen combustion on a Pd based catalyst.[7] They reported 98% approach to equilibrium in 1 ms contact time. In related experimental work,[6] they reported over 90% methane conversion at a contact time of a few ms in a SR channel integrating an adjacent channel with a methane partial oxidation zone followed by a combustion zone.

On the modeling front, there are a few theoretical parametric studies on methane SR in mesoscale reactors in which the smallest characteristic length scale is equal to or higher than $\geq$1 mm.[8–13] With rare exceptions, e.g.,[11,14] empirical kinetics, such as the global rate expressions by Froment and coworkers,[15] have been employed. In the work of Stutz and Poulikakos,[14] the methane partial oxidation process in a single cylindrical channel of a monolith reactor was numerically studied with detailed chemistry. The important effect of the wall material on the maximum temperature, methane conversion and hydrogen yield was underscored. Finally, Eigenberger and coworkers explored different heat-integrated reactor concepts for catalytic reforming, and stressed the importance of appropriate reaction zone overlapping in order to reduce hot spots in the reactor.[16]

Unlike the aforementioned theoretical works where SR was investigated in mesoscale devices, in this work, we study a microscale (submillimeter gap size) multifunctional reactor combining catalytic propane/air combustion on Pt coupled with catalytic methane SR on Rh in alternate (CPR) channels. We perform a parametric study with respect to operating conditions, such as the combustible and reforming stream flow rates as well as with structural parameters, such as the wall material and the channels' gap size. In line with previously published work of our group,[17,18] we aim at providing the experimentalist and reactor designer with guidelines for choosing the aforementioned parameters for optimized microreactor operation. We mark out the attainable operating regimes for self-sustained operation, as well as for optimal operation. Another major contribution of this work pertains to the chemistry employed for the SR process. Unlike published works, in which lumped kinetic models with fitted parameters are used, the analysis here is performed for first time using fundamental chemistry through a newly developed, reduced, kinetic model for SR and WGS.[19] It is remarked that reliable chemistry is essential for determining the feasibility of the process at microscale.

Model Description

Reactor model

A multifunctional microreactor comprising of two alternate planar channels separated by a solid wall, being catalytically coated on the sides, is simulated. A schematic of the simulated domain is shown in Figure 1. On one side of the wall, catalytic propane combustion on Pt takes place. On the other side of the wall, methane SR (along with water-gas shift (WGS)) on Rh takes place. The wall acts as a heat exchanger between the two channels. This is a popular reactor configuration due to its relative simplicity and compactness; it provides flexibility with respect to the choice of catalyst and fuel used in the two channels, and allows for different flow configurations (e.g., co- and countercurrent flow). Herein, we focus on the co-current flow because it allows for self-sustained operation over a wider flow rate regime, as compared to counter-flow mode. In addition, lower reactor temperatures are obtained due to bigger reaction zone overlapping.[17] Our choice of propane (instead of methane) combustion has been based on its higher reactivity and more robust stability, against extinction, guided from previous CFD work.[20] Finally, in[21,22] the interested reader can find informa-

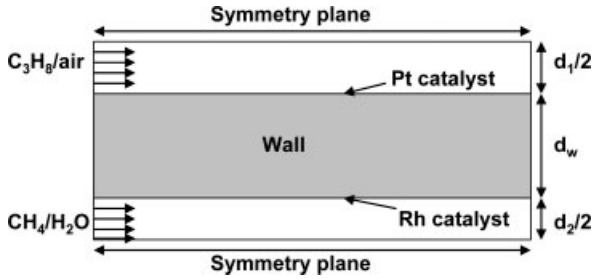

Figure 1. Schematic of the simulated multifunctional microreactor.

tion on how to integrate catalyst layers within stainless steel structured reactors.

A pseudo 2-D reactor model consisting of the mass and the energy balances for the gas-phase in the two channels and the catalytic wall is employed.[23,24] A central Finite Difference scheme is used with 400 axial nodes in each channel. The Sherwood and Nusselt numbers vary with position and can be nonmonotonic. Herein, following recent work, we use constant (average) values of 3.8 and 4.0 that appear suitable for these microreactors.[25] Due to the very high-aspect ratio of the microreactor, radiation is neglected.[26,20] Flow rates, whenever reported, assume a microreactor width (in the third dimension) of 1 cm and are given to provide a sense for real experiments.

Kinetic model

There are several experimental works aiming at the development of lumped kinetic models for SR and WGS on different catalysts.[8,27,28,15] In this work we use lumped reversible rate expressions for methane SR and WGS on Rh, which are based on a reduced microkinetic model. The latter is a product of *a posteriori* reduction of a detailed microkinetic model that has been validated against a number of experimental data,[29] and has recently been revised in reference 30. The reduction of the microkinetic model has been done using principal component analysis and regular perturbation theory. All details on its derivation can be found in[19]. In the following, a reduced kinetic model is given

$$\text{SR: } CH_4 + H_2O \longleftrightarrow CO + 3H_2$$

$$r_{SR} = \frac{k_{55} c_{CH_4}}{\left(1 + \frac{k_{56}}{k_{57}} \sqrt{\frac{k_1}{k_2} c_{H_2}}\right) \left(1 + \sqrt{\frac{k_1}{k_2} c_{H_2}} + \frac{k_{19}}{k_{20}} c_{CO}\right)^2} (1 - \eta_{SR}) \tag{1}$$

where

$$K_{SR} = \frac{p_{CO}\, p_{H_2}^3}{p_{CH_4}\, p_{H_2O}} \tag{2}$$

$$K_{equilibrium,SR} = \exp\left(-\frac{\Delta G_{SR}^0(T)}{RT}\right) \tag{3}$$

$$\eta_{SR} = \frac{K_{SR}}{K_{equilibrium,SR}} \tag{4}$$

$$\text{WGS: } CO + H_2O \longleftrightarrow CO_2 + H_2$$

$$r_{WGS} = \frac{k_7 \frac{k_{13}}{k_{14}} c_{H_2O}}{\left(1 + \sqrt{\frac{k_1}{k_2} c_{H_2}} + \frac{k_{19}}{k_{20}} c_{CO}\right)^2} (1 - \eta_{WGS}) \tag{5}$$

where the equilibrium factor η_{WGS} is defined similarly as for the SR rate expression above.

The concentrations in Eq. 1 and Eq. 5 refer to the surface concentrations. The reaction rate constants (k) in Eq. 1 and Eq. 5 correspond to those reactions of the full microkinetic model that are retained in the reduced microkinetic model. The reduced microkinetic model for the SR and WGS reactions along with the kinetic parameters involved are given in Table 1.

Propane combustion on Pt is modeled as in[31] using a single-step rate expression, which was also developed through *a posteriori* reduction of a microkinetic model that is in

Table 1. Reduced Reaction Mechanism for CH_4 Steam Reforming on Rh

No.	Reaction	Sticking Coefficient (unitless) or Pre-exponentials (s^{-1})	Temperature Exponent β	Activation Energy (kcal/mol)
R_1	$H_2 + 2^* \rightarrow 2H^*$	7.73×10^{-1}	0.939	0.0
R_2	$2H^* \rightarrow H_2 + 2^*$	$5.55 \times 10^{+11}$	1.47	$19.4 - 7.36\,\theta_{CO} - 5.0\,\theta_H$
R_7	$H_2O^* + {}^* \rightarrow H^* + OH^*$	$5.73 \times 10^{+11}$	−0.379	$16.2 - 1.05\theta_H + 15.7\theta_O - 13.4\,\theta_{H_2O} + 28.8\theta_{OH}$
R_{13}	$H_2O + {}^* \rightarrow H_2O^*$	7.72×10^{-2}	1.41	0.0
R_{14}	$H_2O^* \rightarrow H_2O + {}^*$	$2.06 \times 10^{+13}$	−0.757	$10.3 - 4.37\,\theta_{H_2O} + 25.0\theta_{OH}$
R_{19}	$CO + {}^* \rightarrow CO^*$	5.00×10^{-1}	−2.0	0.0
R_{20}	$CO^* \rightarrow CO + {}^*$	$5.65 \times 10^{+12}$	2.88	$38.1 - 15.0\theta_{CO} - 3.7\theta_H$
R_{55}	$CH_4 + 2^* \rightarrow CH_3^* + H^*$	5.72×10^{-1}	−0.441	$10.8 + 1.56\theta_{CO} + 1.05\theta_H$
R_{56}	$CH_3^* + H^* \rightarrow CH_4 + 2^*$	$7.72 \times 10^{+10}$	0.0593	$8.61 - 2.14\theta_{CO} - 1.45\theta_H$
R_{57}	$CH_3^* + {}^* \rightarrow CH_2^* + H^*$	$2.49 \times 10^{+10}$	−0.203	$11.0 + 1.08\theta_{CO} + 0.733\theta_H$

The reaction rate constant (k) is calculated as follows: $k = \frac{A}{\Gamma_{Rh}^{n-1}} \left(\frac{T}{T_0}\right)^{\beta} e^{-E/RT}$ or $k = \frac{S}{\Gamma_{Rh}^{n}} \sqrt{\frac{RT}{2\pi MW}} \left(\frac{T}{T_0}\right)^{\beta} e^{-E/RT}$, where A is the pre-exponential, s is the sticking coefficient, Γ_{Rh} is the site density, n is the reaction order with respect to the surface species, E is the activation energy, R is the ideal gas constant and T_0 is the reference temperature (300 K). In the simulations, Γ_{Rh} has been set equal to 2.49×10^{-9} mol/cm^2. Concerning the coverages, as an approximation, the following values are used (balance vacancies): $\theta_H = 0.25$ and $\theta_{CO} = 0.05$.

Table 2. Kinetic Rate Parameters for Propane Combustion

Reaction	A (s^{-1}) or s (−)	β	E_{act} (kcal/mol)
$C_3H_8+2^* \rightarrow C_3H_7^*+H^*$	0.06	0.154	4.0
$O_2+2^* \rightarrow 2O^*$	0.0542	0.766	0.0
$2O^* \rightarrow O_2+2^*$	$8.41 \times 10^{+12}$	−0.796	$E_{O_2}^{des} = 52.8 - 2.3(T/T_0) - 32.0\theta_o$

The activation energy for oxygen desorption is dependent on the surface coverage of oxygen (θo) and temperature. $T_0 = 300$ K.

good agreement with experimental data (both catalyst ignition and autothermal fixed bed data) under fuel lean conditions.[32] Details on the derivation of the reduced kinetic model can be found in[33]. For the sake of completeness, the model is presented in the following:

Catalytic propane combustion: $C_3H_8 + 5O_2 \rightarrow 3CO_2 + 4H_2O$

$$r_{cat,C_3H_8} = \frac{k_{C_3H_8}^{ads} c_{C_3H_8}}{\left(1 + \sqrt{\frac{k_{O_2}^{ads} C_{O_2}}{k_{O_2}^{des}}}\right)^2} \tag{6}$$

In Eq. 6, the adsorption and desorption rate constants are calculated using the equations in the caption of Table 1, and their values are quoted in Table 2. The activation energy for the oxygen desorption step depends on the temperature and the oxygen surface coverage (see Table 2). The oxygen coverage is computed locally, along the axial direction, by solving the following nonlinear algebraic equation

$$\theta_o = 1 - \frac{1}{\left(1 + \sqrt{\frac{k_{O_2}^{ads} C_{O_2}}{k_{O_2}^{des}}}\right)} \tag{7}$$

The aforementioned expressions hold over typical operating conditions, and do not apply in the limit where one co-reagent is missing. It is remarked here that the full model for the combustion channel (i.e., the reduced combustion chemistry model along with the reactor model described in the previous section) has been successfully validated through (a) CFD results with the commercial package FLUENT in[31,34], and (b) experimental data in[31] in terms of axial wall temperature profiles when using different metal thermal spreaders mounted on the catalytic plate. Since the overall model used in this work builds upon fundamental parts that have been individually validated, it is expected to work reasonably well.

Table 3. Nominal Values of Simulation Variables that are Kept Constant Unless Otherwise Stated

Reactor length	l	5 cm
Wall thickness	d_w	750 μm
Wall conductivity	k_s	15 W/m/K
Combustion channel		
Gap size	d_1	300 μm
Equivalence ratio	ϕ	0.85
Inlet velocity	u_0	6.1 m/s (1 SLPM)
Inlet temperature	T_{in}	300 K
Pressure	P	1 atm
Catalyst to geometric surface area	η	1.7
Steam reforming channel		
Gap size	d_2	200 μm
Inlet composition	S/C	2
Inlet temperature	T_{in}	400 K
Pressure	P	1 atm
Catalyst to geometric surface area	η	1.0

To facilitate the analysis in the ensuing sections, a base case is specified, whose variables are quoted in Table 3, and used for the simulations unless otherwise stated. The inlet in the reforming channel is a methane/water vapor mixture; hence the inlet temperature is assumed to be at 400 K. The points in panels, whenever shown are calculations and the lines just connect the points.

Role of reforming stream flow rate

In this section, the various operating lines are introduced. We have intentionally chosen the combustible stream inlet velocity in the stable operating regime, such that propane conversion is complete in all cases. This eliminates the complication of (additional) extinction and blowout operating lines we have discussed in recent work.[31,23,24,35,20] Figure 2A and B show the wall temperature and methane conversion vs. reactor length for different reforming stream inlet velocities at a constant combustible stream inlet velocity of 6.1 m/s (1 SLPM). In these and subsequent graphs, whenever we display reactor length on the x-axis, we refer to the location from the entrance or axial coordinate of a (total length fixed) 5-cm long reactor. The reforming stream inlet velocity increases from the top to the bottom of the graphs. Herein, the maximum wall temperature always corresponds to the maximum reactor temperature. Figure 2C shows the maximum wall temperature and the methane conversion vs. reforming stream inlet velocity and flow rate. Figure 2D shows the power output vs. reforming stream inlet velocity and flow rate. The power output is computed using the lower heating value of hydrogen at 300 K.

At a relatively low reforming stream inlet velocity of 1.22 m/s (thick solid line), the heat demand for methane conversion is quite lower than the heat released via combustion. Therefore, the wall temperature gets as high as 1,750 K in the post-reforming zone (Figure 2A). Such high-temperatures are undesirable due to material stability issues. The high catalytic reforming rates, due to the high-wall temperatures, drive methane conversion to completion very fast (<0.5 cm, Figure 2b). Increasing the reforming stream inlet velocity, at a constant combustible stream inlet velocity, increases the amount of heat that is converted to chemical energy, due to the endothermic reaction, causing a concomitant decrease in the wall temperature.

At a reforming stream inlet velocity of 2.56 m/s, the wall temperature is slightly below 1,500 K (Figure 2A, dashed line). At this temperature, 100% methane conversion is still achieved within 2.5 cm from the entrance (Figure 2B, dashed line). Like previously published work,[17,18] 1,500 K is a rea-

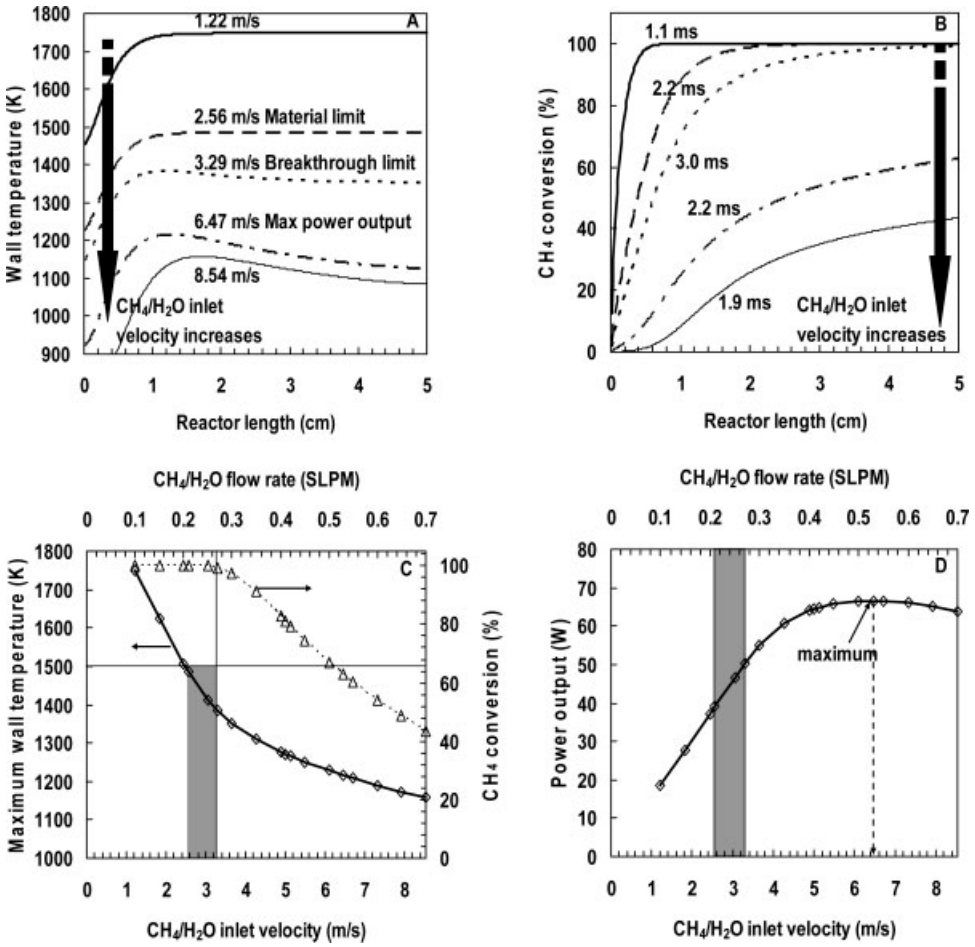

Figure 2. (A) Wall temperature, and (B) CH_4 conversion vs. reactor length for different reforming stream inlet velocities (in (B) same inlet velocities as in (A) are implied for the same line configurations); (C) maximum wall temperature and CH_4 conversion at the outlet vs. reforming stream inlet velocity and flow rate; the vertical line denotes the CH_4 breakthrough limit; the horizontal line denotes the materials stability limit and the shaded region represents the operating region that satisfies both of these conditions; (D) power output vs. reforming stream inlet velocity and flow rate.

The combustible mixture inlet velocity is 6.1 m/s (1 SLPM). The wall thermal conductivity (k_s) is 15 W/m/K.

sonable, yet somewhat arbitrary, upper temperature bound for materials stability. Our choice of the specific temperature of the wall material limit is based on the observation that SR on noble metals appears stable experimentally at high-temperatures and partial oxidation has been conducted at temperatures as high as 1,200 °C.[36,37,4] One could obviously pick a lower temperature and modify slightly the limits of operation, since concepts remain the same.

A methane conversion of 99% is hereafter defined as the breakthrough limit. The breakthrough limit is obtained at a reforming stream inlet velocity of 3.29 m/s (0.27 SLPM-dotted lines). Reforming stream inlet velocities higher than 3.29 m/s, result in incomplete conversion and lower wall temperatures. At a reforming stream inlet velocity of 6.47 m/s (0.53 SLPM), the maximum hydrogen yield is obtained (Figure 2D). The maximum is caused by a trade-off between higher flow rate, but lower conversion (of methane). The maximum wall temperature at the maximum power output limit is reasonable (~1,200 K, Figure 2A, dashed-dotted line), and the methane conversion at the outlet is 63% (Figure 2B, dashed-dotted line; Figure 2C). Further increase in the reforming stream inlet velocity causes further decrease in wall temperatures, methane conversion, and hydrogen outlet flow rate from its maximum value. In Figure 2C, the vertical line denotes the methane breakthrough limit, and the horizontal line denotes the material stability limit. The shaded region, whenever used in this work, represents the operating region that satisfies both of these conditions.

The times in Figure 2B are contact times (t_c) in the reforming channel. In the complete conversion regime, the contact time is calculated as the sum of contact times in each reactor differential up to 99.9% methane conversion (i.e., the contact time in the effective, reactive length of the reactor). In the incomplete conversion regime, the contact time is the sum of contact times in each reactor differential of the entire reactor. The contact times over the entire range

of reforming stream inlet velocities are on the order of a few milliseconds. This implies that both the intrinsic SR chemistry on Rh, as well as transverse mass and heat transfer in the reactor are sufficiently fast to enable SR in microscale (<1 mm characteristic dimension) reactors at millisecond times. Our results are in excellent agreement with a recent experimental report on the same catalyst.[7] In related work, we have found that on Rh the intrinsic speed of SR chemistry is actually comparable to that of partial oxidation (milliseconds); this is not surprising given the fact that partial oxidation, under kinetics-limited conditions, consists of a very short combustion zone followed up by a slower SR zone.[36–38,29]

Reaction zone analysis

Overlap of reaction zones could lead to hot spot elimination and is a potential advantage of the co-current configuration. In this section, we explore this overlap and conditions that maximize it.

Figure 3 shows the locus of locations of the maximum SR rate (solid line with diamond symbols), the maximum propane combustion rate (solid line with square symbols), and the methane conversion (solid line with triangle symbols) over the SR inlet velocity range discussed in Figure 2. The combustible stream inlet velocity is 6.1 m/s (1 SLPM). The shaded region denotes the operating regime between the materials stability limit (left, vertical, solid line) and the breakthrough limit (right, vertical, solid line). The vertical dashed line shows the reforming stream inlet velocity and flow rate at which the maximum hydrogen flow rate at the outlet (and maximum power output) is obtained. Figure 4I-IV show the wall temperature profile, the SR reaction rate profile, the combustion and reforming reaction heat flux profiles, as well as the methane conversion profile for the three designated cases (A, B, and C) of Figure 3.

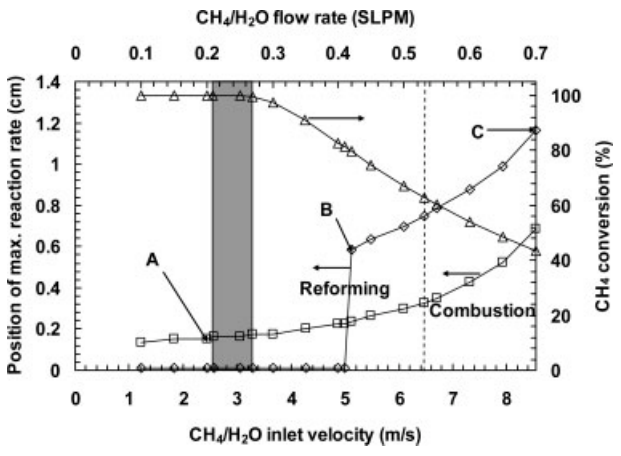

Figure 3. Position of maximum combustion and reforming reaction rates and CH_4 conversion vs. reforming stream inlet velocity and flow rate.

The combustible stream inlet velocity is 6.1 m/s (1 SLPM). The wall thermal conductivity (k_s) is 15 W/m/K. The shaded region represents the operating region that satisfies the materials stability (left vertical solid line), and CH_4 breakthrough (right vertical solid line) requirements. The vertical dashed line indicates the reforming stream inlet velocity and flow rate for which the maximum power output is obtained. Profiles at designated points (A, B, C) are shown in Figure 4.

Figure 3 shows that for low-reforming stream inlet velocities (up to 5 m/s), the maximum reforming rate is anchored just past the entrance. Sufficient heat is generated via combustion, and is transferred fast upstream via wall conduction to stabilize the SR chemistry. The increased heat consumption with increasing reforming stream flow rate results in lower local temperature, and pushes the combustion front slightly downstream. However, over this low-range of flow rates, the combustion and reforming reaction zones remain close to one another and rather close to the inlet. Moreover, the peak combustion rate is always downstream of the peak reforming rate. At ~5.1 m/s, a transition occurs and the maximum reforming rate abruptly moves well downstream of the maximum combustion rate. For even higher reforming stream inlet velocities (and flow rates), the locations of the maximum rates are more sensitive to the reforming stream inlet velocity, and the distance between them is larger. In parallel, the methane conversion decreases substantially. For inlet velocities higher than the breakthrough line, the reaction zones overlap less. However, given that the reaction zones in the two channels are fairly broad, reasonable overlap of reaction zones occurs.

Figure 4 throws some light at the abrupt "jump" of the maximum SR rate location at ~5.1 m/s (Figure 3). Figure 4I shows that at low-reforming stream inlet velocities (case A), the wall temperature is high just past the entrance (~1,250 K at 0.0125 cm). Due to the hot wall and the very high-methane concentration, the SR reaction rate is maximum there and decreases monotonically downstream (Figure 4II). Of course, the maximum SR heat flux is also found at the same point (Figure 4III), and is ~150 kW/m^2. As the reforming stream inlet velocity (and flow rate) increases, the SR reaction rate just past the entrance decreases, and a second local maximum in the rate further downstream develops. This nonmonotonic behavior arises from the concentration and temperature trade-off as one moves downstream past the entrance (decrease in methane concentration and increase in temperature). At the transition SR inlet velocity (5.12 m/s; case B), two reaction rate maxima are distinguished in Figure 4II; one near the entrance, where the wall temperature is high (~1,000 K, Figure 4I), and methane concentration is maximum (conversion approximately 0%, Figure 4IV), and one at ~0.6 cm, where the wall temperature is substantially higher (>1,200 K, Figure 4I), and methane conversion is ~22% (Figure 4IV). As the reforming stream inlet velocity increases even further (curves C), the front end of the reactor cools down (Figure 4I), which in turn lowers the maximum SR rate, as well as the maximum combustion and reforming heat fluxes (Figure 4II and 4III). A single maximum SR rate occurs that moves downstream with increasing reforming stream inlet velocity. It is found that the higher the reforming stream inlet velocity, the wider the SR and combustion reaction zones.

It becomes quite clear that, as found previously in multifunctional gas burners-catalytic microreactors,[17,18] properly balancing flow rates is an important consideration. This balance affects the maximum reactor temperature, and, thus, the conversion and the energy efficiency. A natural question

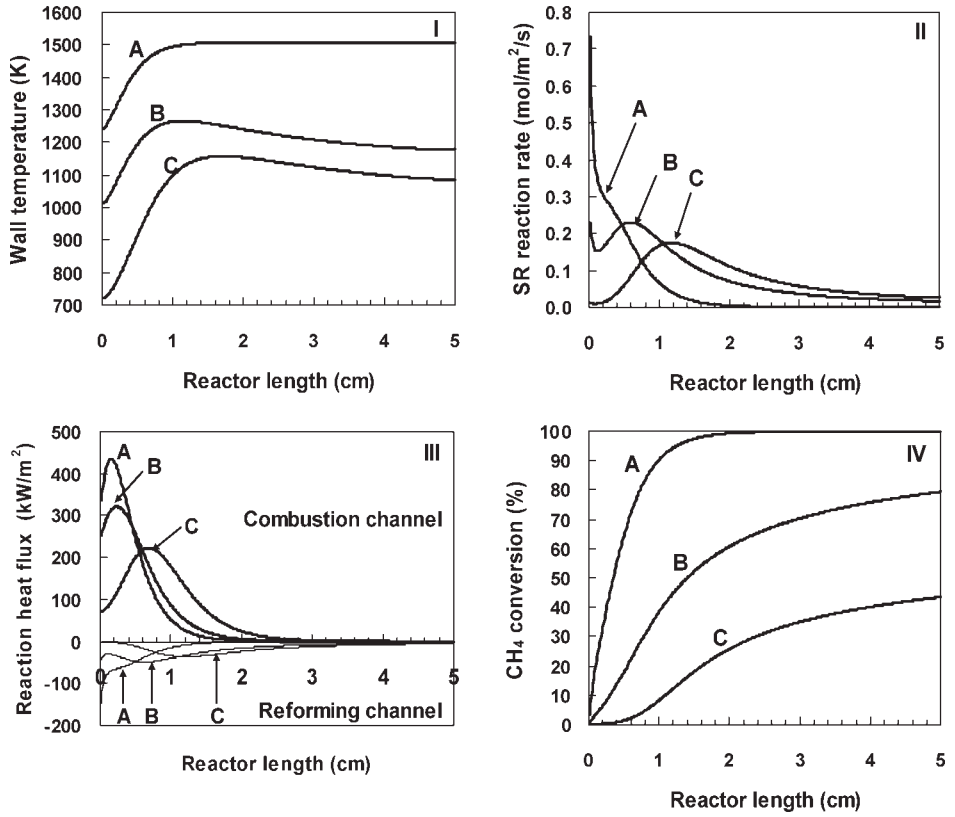

Figure 4. Wall temperature (I), steam reforming (SR) reaction rate (II), reaction heat flux (III), and CH_4 conversion vs. reactor length (IV) for the three designated cases of Figure 3.

raised is how this balance changes with other operating conditions. This is discussed in the following section on attainable regions.

Attainable regions, power output from the microreactor, and efficiency

The aforementioned findings can be generalized by depicting various operating lines as a function of another parameter (e.g., combustible stream inlet velocity and flow rate). Figure 5A shows the locus of maximum wall temperatures along the materials stability line, the breakthrough line, and the maximum power output line. At each constant combustible stream inlet velocity, the reforming stream inlet velocity gradually increases from the top to the bottom of the diagram.

Figure 5B shows the ratio of flow rates in the two channels along the three operating lines. A ratio of reforming to combustible stream flow rates between 0.25 and 0.3 allows operation of the microreactor at or close to the breakthrough limit over a wide range of combustible stream flow rates. The maximum wall temperature under these conditions is always below the selected materials stability limit (<1,450 K).

The aforementioned ratio of flow rates written above is fuel-specific, and is different for different endothermic and exothermic reactions. Furthermore, it is the outcome of repetitive simulations. A general back-of-the-envelope calculation, shown next, provides a good approximation value of the ratio of flow rates at the breakthrough limit for any given combustible and reforming mixtures. For a steady-state process, the overall energy balance on the wall dictates that the net heat generated via the exothermic and endothermic reactions is absorbed as sensible heat in the combustion and reforming channels. This reads

$$y^{in}_{C_3H_8}\dot{m}_1\Delta H_{comb} + y^{in}_{CH_4}\dot{m}_2\Delta H_{ref} + \dot{m}_1\overline{c_{p1}}(T_1^{out} - T_1^{in}) + \dot{m}_2\overline{c_{p2}}(T_2^{out} - T_2^{in}) = 0 \quad (8)$$

Here, y denotes mass fraction, $\dot{m}$ denotes mass flow rate and the subscripts 1 and 2 refer to the combustion and reforming channel, respectively. In Eq. 8, the contribution of the WGS reaction is neglected (the contribution of the WGS reaction is small at normal operating conditions[19]). The average mixture values $\overline{c_p}$ can be approximated as the arithmetic averages of the product mixture c_p values between the inlet and outlet temperature. The heats of reactions are approximated at 300 K. Assuming 100% conversion in both channels at an outlet temperature of 1,400 K, Eq. 8 predicts a ratio of volumetric flow rates: $Q_2/Q_1 = 0.25$ (SLPM/SLPM). Figure 5b, shows that the Q_2/Q_1 ratio at the breakthrough limit (<99% methane conversion) is ~0.3. For an outlet temperature of 1,000 K, Eq. 8 gives $Q_2/Q_1 = 0.46$. With better approximation of the heats of reactions and the specific heats, the predicted ratio of flow rates is more accurate. The most critical factor in this calculation is the outlet reactor temperature.

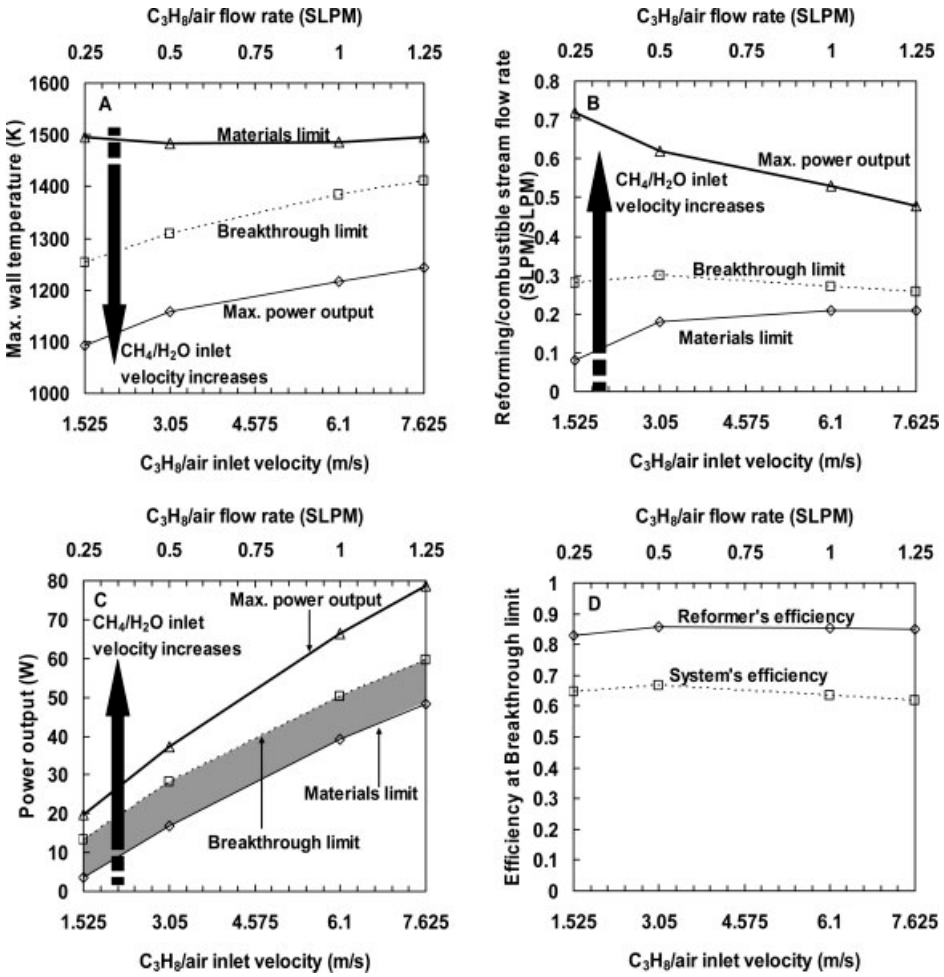

Figure 5. (A) Maximum wall temperature, (B) ratio of reforming stream to combustible stream flow rate, (C) power output, and (D) system's and reformer's efficiency at the breakthrough point vs. combustible stream inlet velocity and flow rate.

However, the estimate is bounded within a factor 2 from the model prediction, even with a poor choice of the outlet temperature. In other words, the energy balance can provide an excellent (back-of-the envelop) estimate of flow rates.

Figure 5C shows the corresponding microreactor power output, defined previously. For the range of combustible stream inlet velocities considered here, the maximum power output (thick, solid line) is obtained when the methane conversion is between 52 and 66%. Several important observations can be made from Figure 5C: First, higher power output can be obtained when the reactor is operated at higher combustible stream inlet velocities (for the range considered). This is because higher combustible stream inlet velocities result in higher heat input, and, thus, they can reform larger flow rates of methane. However, microreactor operation at high-combustible stream inlet velocities is limited from high-wall temperatures. Evidently, at some combustible stream inlet velocity, beyond 7.6 m/s (1.25 SLPM), the breakthrough and the materials stability lines would cross. Furthermore, microreactor operation at high-reforming stream inlet velocities is limited by low-residence times that inevitably lead to incomplete conversion and lower power output. Second, the attainable power output range shrinks at low-combustible stream inlet velocities because the allowable range of reforming stream inlet velocity for a self-sustained process shrinks. Third, the power output calculated is on the order of tens of Watts. Therefore, a stand-alone microreactor can be used for power generation for portable electronics and a few hundred such microreactors stacked together can generate power in the order of tens of kW.

Figure 5D shows the efficiency of the system and of the reforming channel vs. the combustible stream inlet velocity along the breakthrough line of Figure 5c. The system's efficiency, defined as the power output in the form of syngas over the power input in the form of methane and propane on the basis of their lower heating values, is ~65%. The reformer's efficiency, defined as the power output in the form of syngas over the power input in the form of methane and the heat input from the combustion channel, is ~85%. In these definitions, it is assumed that the sensible heat content of the exit streams from the two channels is wasted. In heat integrated systems involving recuperative heat exchange,

the thermal efficiencies will be much higher than the numbers reported here.

Role of channels' gap size

In this section, the parameter under consideration is the reforming and the combustion channel gap sizes, which vary up to 10 times their nominal values. When varying the gap size, one can keep either the flow rates or the velocities fixed.[39] Herein, we have chosen to *keep the reforming and combustible stream flow rates constant* (*close to the desirable breakthrough limit*), since we consider that the power generated (and, thus, the reformer flow rate) will be the primary target in such devices. The flow velocity is inversely proportional to the gap size at a constant flow rate, and, thus, the residence time is proportional to the gap size.

In Figure 6, the power output and the methane conversion are plotted vs. normalized reforming and combustion channel gap sizes with respect to their nominal values. The subscripts 1 and 2 refer to the combustion and reforming channel, respectively. Figure 6 shows that the power output and the methane conversion remain insensitive to the reforming channel gap size change (solid lines). Given the constant flow rates in the two channels, this implies vary fast transverse mass transfer in the reforming channel. Indeed, our calculations have shown that the transverse Damköhler (Da_t) number ranges from ~0.04 for the nominal gap size to ~0.5 for a gap size 10 times the nominal value (the Da_t numbers are representative values calculated at 1 cm from the entrance).

On the other hand, Figure 6 shows that the power output and the methane conversion decrease with increasing combustion channel gap size (dashed lines). For a combustion channel gap size larger than 0.06 cm (twice the nominal value), there is methane breakthrough. Unlike the reforming process, the dominant effect here is the external mass-transfer limitations (despite the longer residence times). Our calculations have shown that Da_t in the combustion channel ranges from ~2 for the nominal gap size to ~10 for a gap size 10 times the nominal value. At the lowest gap sizes examined, the increase in performance is rather small. Thus, it appears that designing sufficiently narrow channels, so that mass-transfer limitations are rather small, is beneficial to power generation. Very narrow channels are undesirable due to increased pressure drops and a higher probability of plugging.

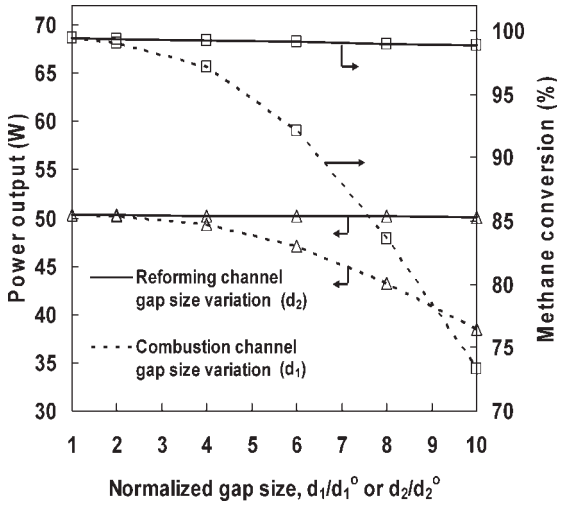

Figure 6. Power output and methane conversion vs. normalized combustion and reforming channel gap size (d_1/d_1° and d_2/d_2°, respectively).

The nominal combustion channel gap size is $d_1^\circ = 0.03$ cm. The nominal reforming channel gap size is $d_2^\circ = 0.02$ cm. The solid lines refer to variation in the reforming channel gap size. The dashed lines refer to variation in the combustion channel gap size. The reforming and combustible stream flow rates are kept constant at 0.27 SLPM and 1 SLPM, respectively (close to the breakthrough limit for the nominal sizes).

Role of wall thermal conductivity

In Figure 7, the effect of the wall material on methane conversion, maximum wall temperature, and power output is investigated. These are plotted vs. reforming stream inlet velocity for three different wall conductivities at a fixed combustible stream inlet velocity of 3.05 m/s (0.5 SLPM). The three wall conductivity values selected are: 3, 15, and 300 W/m/K. The first value represents low conductivity ceramic materials (e.g., cordierite, silica, alumina), the second stainless steel, and the third is a rather high theoretical value representing very conducting materials (e.g., aluminum, copper). Results do not differ for wall thermal conductivities higher than ~100 W/m/K (e.g., silicon carbide, platinum).

The horizontal solid line at 1,500 K specifies the materials stability limit. The vertical solid line specifies the breakthrough limit. The shaded box specifies the region where both conditions are satisfied. Figure 7 shows that at low-reforming stream inlet velocities (up to the vertical line), the wall thermal conductivity affects only the maximum wall temperature and not methane conversion. On the contrary, in the incomplete methane conversion regime (to the right of the vertical line), the wall thermal conductivity affects both the maximum wall temperature and the methane conversion. In particular, the lower the wall thermal conductivity is, the higher the maximum temperature, and the higher the methane conversion. The former effect explains the latter one, since hot spot formation localized in the reforming zone increases the SR reaction rate. The inset of Figure 7 shows that in the incomplete conversion regime, the power output is higher for the lowest conductivity material at a given reforming stream flow rate as a result of the higher methane conversion. Furthermore, the power output increases with increasing reforming stream flow rate for all conductivities up to a maximum value (not shown). The operating region in Figure 7 corresponds to the region below the maximum power output line in Figure 5c.

Figure 8 provides a closer look into the hot spot formation; the wall temperature profiles for the three thermal conductivities are plotted at the breakthrough line. It is shown that use of a high-wall conductivity material (dotted line) results in an isothermal wall. More insulating materials, not only increase the maximum wall temperature, but also cause steep axial temperature gradients, which may be detrimental for the catalyst and the mechanical properties of the wall.

All in all, the gist of the analysis on the role of the wall thermal conductivity is that at low-reforming stream inlet velocities, high-conductivity ceramics or metals are preferred

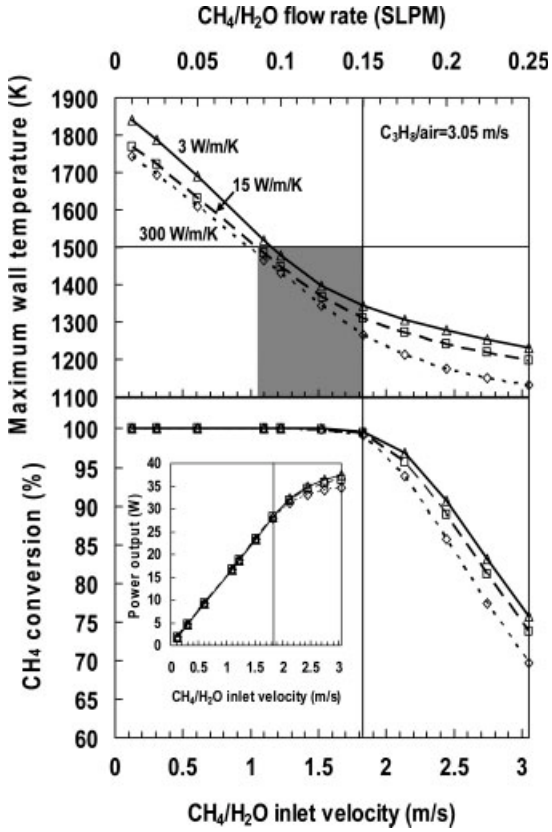

Figure 7. Maximum wall temperature and CH_4 conversion vs. reforming stream inlet velocity and flow rate at a constant combustible stream inlet velocity of 3.05 m/s (0.5 SLPM) for various wall thermal conductivities.

The vertical line denotes the CH_4 breakthrough limit; the horizontal line denotes the materials stability limit, and the shaded region represents the operating region that satisfies both of these conditions for a wall thermal conductivity (k_s) of 15 W/m/K. The inset shows the power output from the microreactor vs. reforming stream inlet velocity.

to low-conductivity ceramic materials, because they smooth out temperature gradients while methane conversion is complete. On the contrary, if the overall economics of the system suggest reactor operation at the incomplete conversion regime (e.g., at the maximum power output limit), then low-conductivity ceramics will give higher conversion at the risk of hot spot formation and steep temperature gradients.

Proposed operation strategy for variable power generation

Variable power generation is an important practical consideration and requires process tunability over a certain range. The discussion in Figure 5 and the energy balance provide a simple procedure for optimal microreactor operation with variable power output (over a five- to 10-fold range) whose steps are presented in the following.

• Use the energy balance to derive an approximate ratio of the reforming to combustible stream flow rate close to the breakthrough limit for chosen fuels and oxidants. For that, a choice of outlet temperature is required. Our simulations have revealed (Figure 5a) that an outlet temperature of 1,300 K is an appropriate choice over a wide range of flow rates. Reforming flow rates up to (or even a little above) the breakthrough point ensure good overlap of reaction zones (Figure 3).

• Given the ratio of reforming and combustible stream flow rates (obtained above), one can dial in the desired power output by adjusting the flow rates in almost a linear fashion (while keeping the flow rates ratio fixed - *an iso-flow rates ratio strategy*). This procedure corresponds to microreactor operation along the dashed line of Figure 5c (along or close to the breakthrough line).

• There are practical maximum and minimum limits of generated power per single pair of parallel plate reactors. As mentioned before, the maximum allowable combustible stream flow rate, and, subsequently, the maximum power output from a single device are dictated by the materials stability limit due to high-temperatures. Under other conditions, one may also encounter the blowout limit of the combustible stream (not observed herein). The minimum set of flow rates is dictated by heat losses to the environment that would cause device extinction. Finally, mass flow controllers have to be tuned over the desirable range of inlet flow rates. By finding the maximum flow rates and power, one can set the mass flow controllers to reduce the power down to the lowest controllable flow rate limit.

• Aside from the adjusting flow rates, the total generated power can further be adjusted in the desired range by choosing an appropriate number of microreactors stacked together.

• Regarding designing a system, dimensions have to be picked to minimize mass transfer limitations. Taking the combustion channel as an example, whose intrinsic chemistry is typically faster, one can set the transverse Damköhler number equal to 2, assume a temperature (e.g., 1,300 K) and inlet concentrations to estimate the reaction rate, and finally estimate the gap size from $Da_t = 2$.

• Materials of construction depend on what the overall system optimum may be; medium conductivity materials

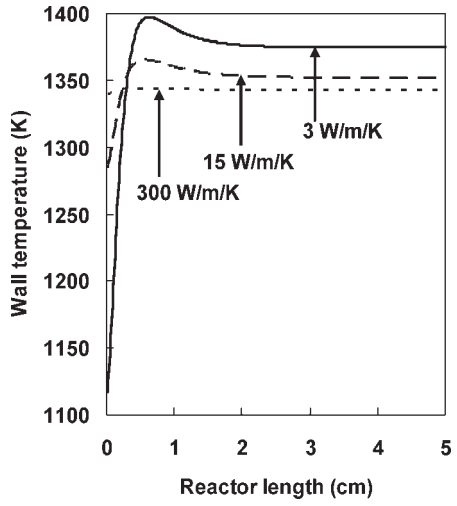

Figure 8. Wall temperature vs. reactor length at the breakthrough line of Figure 7 (vertical line) for three different wall conductivities.

may be a good compromise to minimize hot spots and achieve high-conversions.

Conclusions

Coupled propane combustion/methane steam reforming in a catalytic plate microreactor has been theoretically investigated using fundamental chemistry for both processes with a pseudo 2-D reactor model. Following is a compilation of the major findings:

- Running steam reforming on Rh at microscale at millisecond contact times is feasible. In fact, the process can be designed to operate at submillisecond contact times.[39]
- An operation strategy for a multifunctional microcombustor/microreformer to obtain variable power output has been proposed. According to it, an approximate ratio of the reforming to combustible stream flow rates, close to the breakthrough limit, can be estimated using the overall energy balance with reasonable approximations. Since this ratio does not significantly change with operating flow rates, one can adjust the flow rates (*operation along an iso-flow rate ratio*) to get the desired power output. Along this line, good overlap of reaction zones occurs (Figure 3). The power output from a single device is on the order of some tens of Watts. The maximum power output is limited by the materials stability limit (blowout issues may also occur under certain conditions).
- Reactor sizes must be carefully chosen to minimize mass-transfer effects, but avoid high-pressure drop and plugging. The steam reforming process is reaction-controlled at microscale. Rather, the combustion process timescale is determined from both mass transfer and reaction. Therefore, in order to maximize power output, a combustion channel gap size lower than 600 μm is required. More generally, the gap size can be estimated from $Da_t = 2$.
- Use of low-conductivity wall materials, as opposed to high-conductivity materials, increases fuel conversion and power output in the incomplete conversion regime at the expense of increased maximum wall temperature and axial wall temperature gradients. The differences are more pronounced at lower conversions. Very low-conductivity materials should be avoided since, aside from large temperature gradients, they limit heat transfer upstream and can cause combustion blowout.[31] The final wall material choice depends on the targeted operating regime. If this is the breakthrough point, then intermediate conductivity materials, such as stainless steel, offer a good trade-off between temperature and conversion.

In a follow up article,[40] we compare different combustion fuels and reforming catalysts to provide further design criteria for the operation of multifunctional devices. Further process intensification tips are also discussed. Finally, in Referance 39, we analyze the role of two additional parameters (not studied here), namely the catalyst loading and the inlet steam to carbon ratio, along with a more detailed analysis of the gap size effect; these are important knobs to an experimentalist.

Acknowledgments

This work was supported in part by the NSF (CBET-0729714).

Literature Cited

1. Rostrup-Nielsen J. Steam reforming of hydrocarbons. A historical perspective. In: *Natural Gas Conversion VII*. 2004:121–126.
2. Rostrup-Nielsen T. Manufacture of hydrogen. *Catal. Today*. 2005; 106(1–4):293–296.
3. Trimm DL, Onsan ZI. Onboard fuel conversion for hydrogen-fuel-cell-driven vehicles. *Catal Rev*. 2001;43(1&2):31–84.
4. Venkataraman K, Wanat EC, Schmidt LD. Steam reforming of methane and water-gas shift in catalytic wall reactors. *AIChE J*. 2003;49(5):1277–1284.
5. Holladay JD, Wang Y, Jones E. Review of developments in portable hydrogen production using microreactor technology. *Chem Rev*. 2004;104:4767–4790.
6. Tonkovich AY, Perry S, Wang Y, Qiua D, LaPlante T, Rogers WA. Microchannel process technology for compact methane steam reforming. *Chem Eng Sci*. 2004;59:4819–4824.
7. Tonkovich AY, Yang B, Perry ST, Fitzgerald SP, Wang Y. From seconds to milliseconds to microseconds through tailored microchannel reactor design of a steam methane reformer. *Catal Today*. 2007; 120:21–29.
8. Barrio VL, Schaub G, Rohde M, Rabe S, Vogel F, Cambra JF, Arias PL, Gumez MB. Reactor modeling to simulate catalytic partial oxidation and steam reforming of methane. Comparison of temperature profiles and strategies for hot spot minimization. *Int J Hydrogen Energy*. 2007;32(10–11):1421–1428.
9. Dixon AG, Taskin ME, Stitt EH, Nijemeisland M. 3D CFD simulations of steam reforming with resolved intraparticle reaction and gradients. *Chem Eng Sci*. 2007;62(18–20):4963–4966.
10. Mei H, Li CY, Ji SF, Liu H. Modeling of a metal monolith catalytic reactor for methane steam reforming-combustion coupling. *Chem Eng Sci*. 2007;62(16):4294–4303.
11. Robbins FA, Zhu H, Jackson GS. Transient modeling of combined catalytic combustion/CH_4 steam reforming. *Catal Today*. 2003; 83:141–156.
12. Yuan JL, Ren F, Sunden B. Analysis of chemical-reaction-coupled mass and heat transport phenomena in a methane reformer duct for PEMFCs. *Int J Heat & Mass Trans*. 2007;50 (3–4):687–701.
13. Zanfir M, Gavriilidis A. Catalytic combustion assisted methane steam reforming in a catalytic plate reactor. *Chem Eng Sci*. 2003; 58(17):3947–3960.
14. Stutz MJ, Poulikakos D. Effects of microreactor wall heat conduction on the reforming process of methane. *Chem. Eng Sci*. 2005; 60(24):6983–6997.
15. Xu JG, Froment GF. Methane steam reforming, methanation and water-gas shift.1. Intrinsic kinetics. *AIChE J*. 1989;35(1):88–96.
16. Kolios G, Gritsch A, Morillo A, Tuttlies U, Bernnat J, Opferkuch F, Eigenberger G. Heat-integrated reactor concepts for catalytic reforming and automotive exhaust purification. *Appl Catal B-Environ*. 2007;70(1–4):16–30.
17. Deshmukh SR, Vlachos DG. CFD simulations of coupled, countercurrent combustor/reformer microdevices for hydrogen production. *Ind Eng Chem Res*. 2005;44(14):4982–4992.
18. Deshmukh SR, Vlachos DG. Effect of flow configuration on the operation of coupled combustor/reformer microdevices for hydrogen production. *Chem Eng Sci*. 2005;60(21):5718–5728.
19. Maestri M, Vlachos DG, Beretta A, Groppi G, Tronconi E. Steam and dry reforming of methane on Rh: Microkinetic analysis and hierarchical kinetic models. *J Catal*. 2008;259:211–222.
20. Norton DG, Vlachos DG. A CFD study for propane/air microflame stability. *Combust. Flame*. 2004;138:97–107.
21. Federici J, Vlachos DG. Single channel and heat recirculation catalytic microburners: An experimental and computational fluid dynamics study. *Proc. Combust. Inst*. 2008:in press.
22. Karim A, Federici J, Vlachos DG. Portable power production from methanol in an integrated thermoeletric/microreactor system. *J Power Sources*. 2008;179:113–120.
23. Kaisare NS, Vlachos DG. Extending the region of stable homogeneous micro-combustion through forced unsteady operation. *Proc Combust Inst*. 2007;31(2):3293–3300.
24. Kaisare NS, Vlachos DG. Optimal reactor dimensions for homogeneous combustion in small channels. *Catal Today*. 2007;120(1):96–106.

25. Kaisare N, Stefanidis GD, Vlachos DG. Transport Phenomena in Microscale Reacting Flows. In: *Handbook of Microprocess Engineering: Fundamentals, Operations, and Catalysts*. Renken A, Wang Y, ed. Wiley-VCH: Berlin; 2007 in press.
26. Kaisare NS, Lee JH, Fedorov AG. Hydrogen generation in a reverse flow microreactor: 1. Model formulation and scaling. *AIChE J*. 2005;51(8):2254–2264.
27. Hou KH, Hughes R. The kinetics of methane steam reforming over a Ni/alpha-Al_2O_3 catalyst. *Chem Eng J*. 2001;82(1–3):311–328.
28. Tavazzi I, Maestri M, Beretta A, Groppi G, Tronconi E, Forzatti P. Steady-state and transient analysis of a CH4-catalytic partial oxidation reformer. *AIChE J*. 2006;52(9):3234–3245.
29. Mhadeshwar AB, Vlachos DG. Hierarchical multiscale mechanism development for methane partial oxidation and reforming, and for thermal decomposition of oxygenates on Rh. *J Phys Chem B*. 2005;109:16819–16835.
30. Maestri M, Vlachos DG, Beretta A, Groppi G, Tronconi E. A C1 microkinetic model for methane conversion to syngas on Rh. AIChE J. 2008:accepted.
31. Kaisare NS, Deshmukh SR, Vlachos DG. Stability and performance of catalytic microreactors: Simulations of propane catalytic combustion on Pt. *Chem Eng Sci*. 2008;63(4):1098–1116.
32. Mhadeshwar AB. *A Hierarchical multiscale modeling approach for predictive microkinetic modeling of hydrogen production*. University of Delaware; 2005. PhD Thesis.
33. Deshmukh S, Vlachos DG. A reduced mechanism for methane and one-step rate expressions for fuel-lean catalytic combustion of small alkanes on noble metals. *Combust Flame*. 2007;149(4):366–383.
34. Stefanidis GD, Vlachos DG. Modeling ignition in catalytic microreactors. *Chem Eng Technol*. 2008;31(8):1170–1175.
35. Norton DG, Vlachos DG. Combustion characteristics and flame stability at the microscale: A CFD study of premixed methane/air mixtures. *Chem Eng Sci*. 2003;58:4871–4882.
36. Horn R, Williams KA, Degenstein NJ, Bitsch-Larsen A, Nogare DD, Tupy SA, Schmidt LD. Methane catalytic partial oxidation on autothermal Rh and Pt foam catalysts: Oxidation and reforming zones, transport effects, and approach to thermodynamic equilibrium. *J Catal*. 2007;249(2):380–393.
37. Horn R, Williams KA, Degenstein NJ, Schmidt LD. Mechanism of H_2 and CO formation in the catalytic partial oxidation of CH4 on Rh probed by steady-state spatial profiles and spatially resolved transients. *Chem Eng Sci*. 2007;62(5):1298–1307.
38. Maestri M, Tronconi E, Groppi G, Vlachos DG. Partial oxidation of methane on Rh: Modeling reveals direct vs. indirect pathways. 2008:in preparation.
39. Stefanidis GD, Vlachos DG. Millisecond methane steam reforming via process and catalyst intensification. *Chem Eng Technol*. 2008;31(8):1201–1209.
40. Stefanidis GD, Vlachos DG. Intensification of steam reforming of natural gas: Choosing combustible fuel and reforming catalyst., Chem Eng Sci. 2008 submitted.

Manuscript received Mar. 28, 2008, and revision received July 16, 2008.